Doping-independent 120° magnetism in the quadruple perovskite CaMn3V4O12

Fabio Denis Romero, Kunlang Ji, Claire Colin, J. Paul Attfield

Doping-independent 120° magnetism in quadruple perovskite $CaMn_3V_4O_{12}$

Fabio DENIS ROMERO,[1*] Kunlang JI,[2] Claire V. COLIN,[1] J. Paul ATTFIELD[2]

1. Université Grenoble Alpes
   CNRS
   Institut Néel
   38000 Grenoble
   France
2. Center for Science at Extreme Conditions
   The University of Edinburgh
   Edinburgh EH9 3FD
   United Kingdom

* fabio.denis-romero@neel.cnrs.fr

Abstract

The magnetic structure of high-pressure quadruple perovskite $CaMn_3V_4O_{12}$ was investigated using neutron powder diffraction data. Below T_N = 54 K, the S = 5/2 Mn^{2+} spins adopt a 120 ° arrangement in kagomé layers formed of second nearest neighbor A' sites. The V^{4+} electrons are itinerant and do not mediate the magnetic interactions as evidenced by the insensitivity of the magnetic structure to the valence of the vanadium cations in the $AMn_3V_4O_{12}$ (A = La^{3+}, Ca^{2+}).

Introduction

The quadruple perovskite structure with general formula $AA'_3B_4O_{12}$ is a particular variant of the cubic perovskite structure which is capable of accommodating magnetic transition metal cations in the square-planar A' sites and octahedral B sites. These materials can show a wide range of interesting properties such as intersite charge transfer, Kondo physics, or Fermi liquid behavior with only minor structural variations. [1–3]

Of particular interest are quadruple perovskite materials without localized B-site cation spins (when B is non-magnetic or with itinerant electrons). As a result of several competing (comparable) interactions between the square-planar A' sites, a wide variety of unusual magnetic structures can be stabilized, such as the collinear G-like antiferromagnetic structure of $CaCu_3Ti_4O_{12}$, the different orthogonal orderings of $CaM_3Ti_4O_{12}$ (M = Fe, Co), or the multi-k ordering of $CaCo_3V_4O_{12}$. [4–9] The wide variety of magnetic structures can be rationalized as originating from the need to minimize the geometric frustration in the kagomé lattices formed by the A' sites along the body diagonal directions of the cubic structure. [7]

The quadruple perovskite $LaMn^{2+}{}_3V^{3.75+}{}_4O_{12}$ offers the clearest visualization of the influence of these layers on the magnetic properties. Below $T_N \sim 44$ K, the Mn^{2+} spins adopt a 120 ° order within planes perpendicular to the cubic <111> direction. [5] The isostructural A-site substituted material $CaMn^{2+}{}_3V^{4+}{}_4O_{12}$ has a transition at $T_N = 54$ K to an "antiferromagnetic state," but the magnetic structure has never been investigated. [10]

In these materials the substitution of Ca^{2+} for La^{2+} changes the valence state of the vanadium cations from +3.75 to +4. [10] In both materials, the A' sites are exclusively occupied by $S = 5/2$ Mn^{2+} cations. [10] In this paper we report the magnetic properties and structure of $CaMn^{2+}{}_3V^{4+}{}_4O_{12}$ determined from neutron powder diffraction.

Experimental

Samples of $CaMn_3V_4O_{12}$ were prepared from a suitable stoichiometric mixture of CaO (99.99%), MnO (99.99%), V_2O_3 (99.99%), and V_2O_5 (99.95%). The precursor powders were ground together using an agate mortar and pestle in an argon-filled glove box and placed inside platinum capsules. These were treated at 900 °C for 30 minutes under 9 GPa using a Walker-type multi anvil press. The pressure was released slowly after quenching to room temperature. Laboratory X-ray powder diffraction were collected using a Bruker D8 diffractometer.

Magnetization measurements were performed using a Quantum Design MPMS-XL SQUID magnetometer. Neutron powder diffraction measurements were carried out using the D1b diffractometer at the ILL neutron source in Grenoble, France from a sample contained in a vanadium can. A monochromatic neutron beam with a wavelength of 2.52 Å was obtained with a HOPG monochromator. In order to have sufficient material for significant neutron scattering, the products of 6 different synthesis runs were combined to yield a total mass of approximately 180 mg. Rietveld refinements of the nuclear and magnetic structures were carried out using the GSAS-II program and magnetic structure determination was performed using k-SUBGROUPSMAG implemented therein. [11,12]

Results

Laboratory X-ray powder diffraction data confirmed the formation of cubic (space group $Im\bar{3}$) $CaMn_3V_4O_{12}$. Zero field and field-cooled magnetization measurements contained a local maximum at $T \sim 54$ K, consistent with previous reports (Figure 1 (a)). [10] A fit of the zero-field cooled data to the Curie-Weiss law in the range 100-300 K yielded values of C = 11.73 emu K / mol and θ = -101.64 K, consistent with previous reports and spin-only $S = 5/2$ Mn^{2+}. [10]

Neutron powder diffraction data collected from $CaMn_3V_4O_{12}$ at 100 K, significantly above the magnetic transition temperature, could be well accounted-for using the cubic quadruple perovskite structure reported previously (wRp = 2.69 %). [10] Observed, calculated, and difference plots are shown in Figure 3 (a) and the refined structural parameters are given in Table 1. Attempts to vary the A' and B site occupancies did not result in any noticeable improvement to the fit, indicating the lack of any significant antisite disorder in this material.

Neutron powder diffraction data collected from $CaMn_3V_4O_{12}$ at 1.5 K contained additional reflections relative to the data collected at 100 K. These could be indexed on the basis of a magnetic propagation vector k = [0, 0, 1]. The data were well accounted-for using the $R\bar{3}$ structure shown in Figure 2 (b). This magnetic cell is related to the nuclear cell by the transformation ($a_m = a_n - c_n, b_m = b_n + c_n, c_m = a_n - b_n + c_n$).

This magnetic structure is the same as that previously reported for $LaMn_3V_4O_{12}$. [5] It consists of Mn spins arranged at 120 ° within the kagomé planes formed by the A' sites along the <111> directions of the cubic nuclear cell (see Figure 2). The refinement of the magnetic structure was carried out using only a single parameter (M_X) and yielded a moment per Mn site of 4.42 μ_B (c.f. 4.17(4) in $LaMn_3V_4O_{12}$), a good match for the $S = 5/2$ Mn^{2+} (wRp = 3.34%). [5] Observed, calculated, and difference plots are shown in Figure 3 (b) and the refined structural parameters are given in Table 2. No evidence of peak splitting or broadening could be observed in the nuclear reflections, indicating that the cubic symmetry of the nuclear cell persists down to the lowest temperature measured.

Neutron powder diffraction data were collected at several other temperatures. A plot of the refined ordered moment as a function of temperature is shown in Figure 1 (b). A fit of these data to the phenomenological power law based on Landau theory of the form $I = A\left(1 - \left(\frac{T}{T_N}\right)^{\alpha}\right)^{\beta}$ with T_N = 54 K yields values of A = 4.27 μ_B, α = 1.77, and β = 0.333, in accordance with the value expected for a classical Heisenberg 3D model (β = 0.367).

$CaMn_3V_4O_{12}$ – 100 K					
Atom	***x***	***y***	***z***	**frac**	**U_{iso} (Å²)**
Ca1	0	0	0	1	0.007
Mn1	0	1/2	1/2	1	0.007
V1	1/4	1/4	1/4	1	0.007
O1	0	0.197(1)	0.297(1)	1	0.007
Space group: $Im\bar{3}$, a = 7.404(1) Å					

Table 1: Parameters for the nuclear structure of $CaMn_3V_4O_{12}$ refined against neutron powder diffraction data collected at 100 K.

$CaMn_3V_4O_{12}$ – 1.5 K					
Atom	***x* / M_x**	***y* / M_y**	***z* / M_z**	**frac**	**U_{iso} (Å²)**

Ca1	0	0	0	1	0.005
Mn1	1/2	0	0	1	0.005
	4.42(1)	0	0		
V1	1/2	0	1/4	1	0.005
V2	0	0	1/4	1	0.005
O1	0.966(1)	0.230(1)	0.034(1)	1	0.005
O2	0.835(1)	0.969(1)	0.164(1)	1	0.005
Space group: $R\bar{3}$ Space group: $R\bar{3}$, a = 10.425(1) Å, c = 12.864(1) [Pseudocubic a = 7.402(1) Å]					

Table 2: Parameters for the nuclear and magnetic structures of $CaMn_3V_4O_{12}$ refined against neutron powder diffraction data collected at 1.5 K.

Discussion

At T_N = 54 K, $CaMn_3V_4O_{12}$ adopts a magnetic structure in space group $R\bar{3}$ with the Mn^{2+} spins lying in kagomé planes parallel to the *ab* plane (perpendicular to the cubic <111> body diagonal of the nuclear cell). These are made up of networks of second nearest neighbor (2NN) A' cations. An equivalent 2NN exchange path exists between next-nearest kagomé layers, while adjacent kagomé layers are instead linked by third nearest neighbor (3NN) interactions. In quadruple perovskite materials, first, second, third, and fourth nearest neighbor exchange interactions are typically comparable in energy, which contributes to the variety of non-trivial types of ordering seen in these phases. It has been noted previously that these structures are all different ways of relieving the inherent geometric frustration present in kagomé layers with AFM interactions. [7]

For the collinear G-like magnetic structures of $CaCu_3Ti_4O_{12}$ or $YMn_3Al_4O_{12}$, the spins within each layers are ferromagnetically aligned and adjacent layers couple antiferromagnetically. [7,13,14] This situation is realized when the interaction between 1NN spins is AFM and the interaction between 2NN is negligible ($J_1 < 0, J_2 \sim 0$). However, when the interaction between 2NN is AFM (i.e. $J_2 < 0$), we observe much more complex arrangements of spins. The 120° arrangement of spins within each layer observed in $AMn_3V_4O_{12}$ (A = La, Ca) is compromise solution.

One additional feature of quadruple perovskites worth considering is the orbital polarization of the A' sites. Interactions between sites with the same orbital polarization (orientation of the O_4 square planar coordination environment) will be more significant than those between sites with orthogonal polarizations. In this structure type, 1NN and 2NN A' sites are orthogonally arranged, while 3NN and 4NN sites are parallel. This stabilizes, for example, the orthogonal order in $CaM_3Ti_4O_{12}$ which have long range structures consisting of three mutually orthogonal AFM sublattices each of which consists of the set of MO_4 square planes sharing a particular orientation. [6,7] In both cases, it is the long range 4NN interaction which is responsible for stabilizing the overall magnetic arrangement.[6,7]

It should be noted that in this case, all Mn^{2+} sites which share a common orientation have colinear ordering Figure 2 (c). All 3NN interactions are AFM and all 4NN interactions are FM. In the resulting structure, thus, only the 2NN interaction is frustrated.

The magnetic structure reported herein is the same as that previously reported for the analogous material $LaMn_3V_4O_{12}$. The substitution of Ca for La results in an change in the average oxidation state of the V cations from +3.75 to +4. [10] This change has minimal effect on the magnetic

properties and both compounds have comparable T_N (44 K and 54 K for La and Ca respectively) and ordered moments (4.17 μ_B and 4.42 μ_B). [10]

The T_N changes from 44 K to 54 K, a change which is largely associated with a decrease in the unit cell volume on substitution (a_{La} = 7.48485(4) Å, a_{Ca} = 7.40704(3) Å at 300 K). [10] In both compounds, the vanadium electrons are itinerant, giving rise to metallic conduction, and do not interact with the localized electrons at the Mn^{2+} sites. The lack of correlation between the magnetic and transport behavior in this family of materials opens up intriguing possibilities to tune different emergent properties independently.

The other reported members of the $CaM_3B_4O_{12}$ are summarized in Table 3. While there are a number of oxides known with Ni^{2+} cations in square planar environments, there are yet no examples of quadruple perovskite materials with Ni^{2+} at the A' sites. This is likely because of the high stability of NiO (and consequent unreactivity) at the high pressures typically required to stabilize these phases. Similarly, attempts to prepare $CaMn_3Ti_4O_{12}$ have so far resulted in the preferential formation of a mixture of $CaTiO_3$ and $MnTiO_3$ perovskites. [15] Attempts to prepare $CaFe_3V_4O_{12}$ at pressures $P \leq 8$ GPa produced a mixture of $(Fe/V)_2O_3$ and $CaVO_3$ while the solid solution limit for the system $CaCu_{3-x}Fe_xV_4O_{12}$ under these conditions is limited to $x \sim 1$. [16]

$CaM_3B_4O_{12}$ M =	$B = V^{4+}$	$B = Ti^{4+}$
Mn^{2+}	T_N = 54 K 120° order k = (0, 0, 1) Metallic [10] (This work)	Not reported
Fe^{2+}	Not reported	T_N = 2.8 K Orthogonal AFM (k = (½, ½, 0)) [6] Insulator
Co^{2+}	T_N = 100 K Multi-k ordering [8,9] k = (0, 0, 1) and (0, 0, ½) Semimetal	T_N = 9.3 K Orthogonal AFM (k = (½, ½, ½)) [7] Insulator
Ni^{2+}	Not reported	Not reported
Cu^{2+}	Pauli paramagnet [17] Metallic	T_N = 27 K G-like AFM [4] k = (0, 0, 0) Insulator

Table 3: Selected magnetic and transport properties of the $CaM_3B_4O_{12}$ materials ($B = V^{4+}, Ti^{4+}$).

Conclusions

We carried out neutron powder diffraction measurements on $CaMn^{2+}{}_3V^{4+}{}_4O_{12}$ and determined its magnetic structure, finding a 120 ° arrangement as in $LaMn^{2+}{}_3V^{3.75+}{}_4O_{12}$ rather than the G-like arrangement found in $CaCu_3Ti_4O_{12}$ previously assumed. [18,19] The low temperature magnetic behavior of these phases is independent of the average vanadium oxidation state, with only a change in T_N ascribable to chemical pressure exerted by a decrease in the lattice parameter. The lack of correlation between the magnetic and transport behavior in this family of materials opens

up intriguing possibilities to tune different emergent properties independently via site-selective doping.

Acknowledgements

K. Ji and JPA acknowledge financial support from EPSRC and access to ILL provided by STFC.

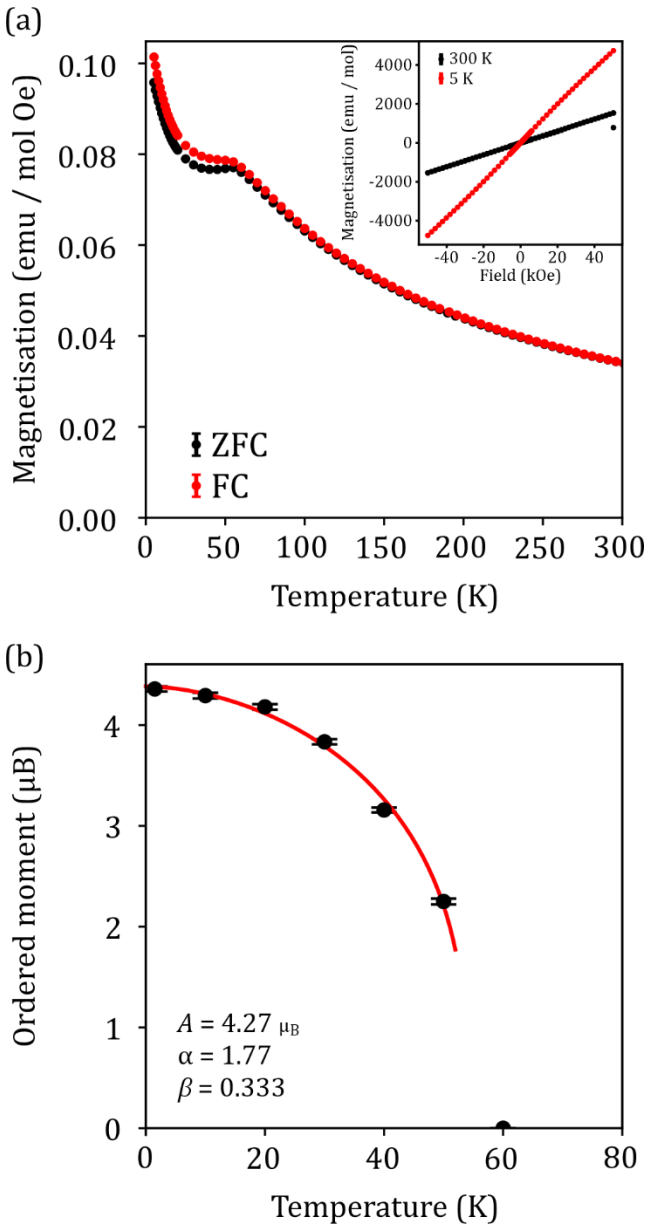

Figure 1: (a) Zero-field (ZFC) and field cooled (FC) magnetisation data collected as a function of temperature from $CaMn_3V_4O_{12}$. Inset: Magnetisation as a function of field at 300 K and 5 K. (b) Refined moment per Mn^{2+} cation as a function of temperature and the fit to a power law of the form $\boldsymbol{I = A\left(1 - \left(\frac{T}{T_N}\right)^{\alpha}\right)^{\beta}}$ with T_N = 54 K.

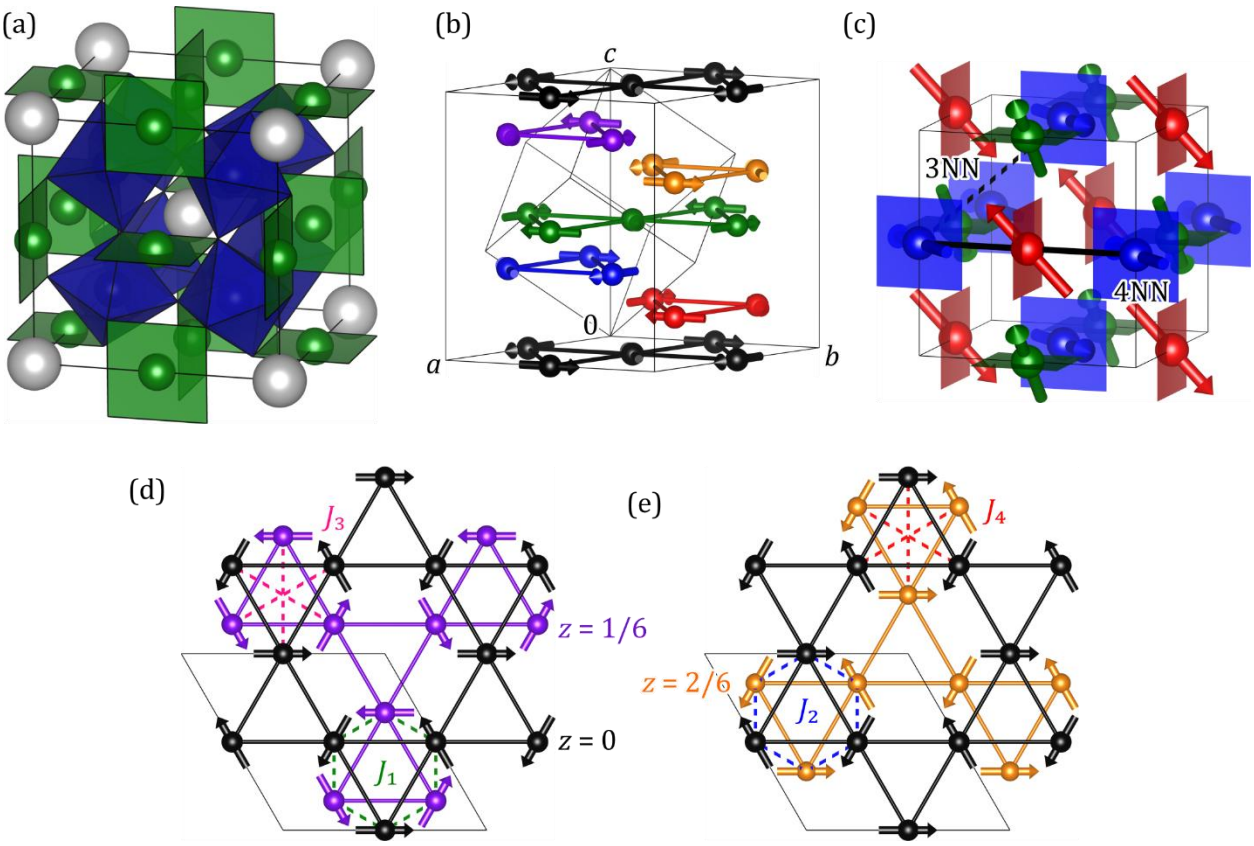

Figure 2: (a) Nuclear structure of $CaMn_3V_4O_{12}$. (b) Rhombohedral magnetic structure of $CaMn_3V_4O_{12}$. The different colors correspond to the different kagomé layers parallel to the rhombohedral *ab* plane. The cell edges of the original nuclear cubic cell are included. (c) Magnetic structure of $CaMn_3V_4O_{12}$ in the cubic setting highlighting the collinear ordering between spins which share a common orientation of the square planar coordination environment. (d) Relation between two 1NN kagomé planes along the <111> direction of the cubic nuclear cell. (e) Relation between two 2NN kagomé planes along the <111> direction of the cubic nuclear cell.

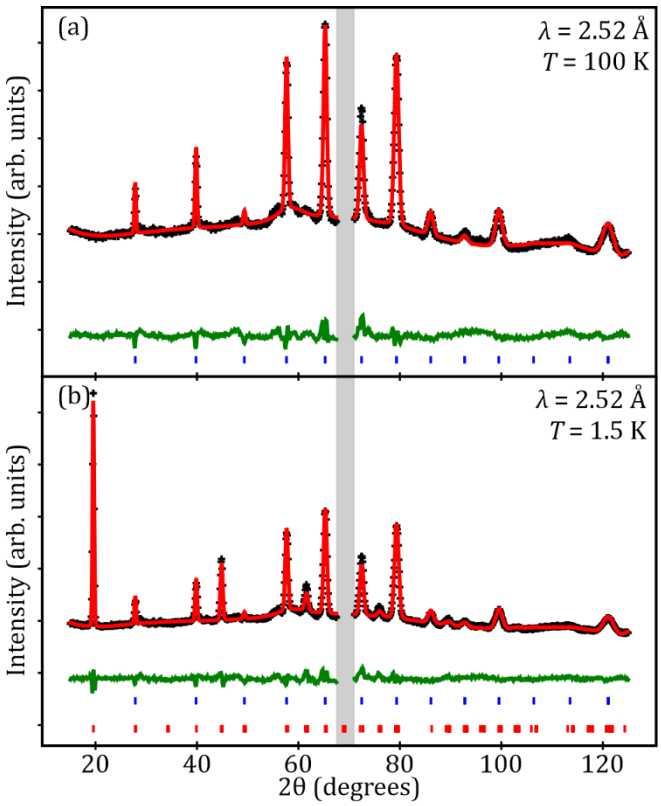

Figure 3: Observed (black), calculated (red), and difference (green) plots for the refinements of $CaMn_3V_4O_{12}$ at (a) 100 K and (b) 1.5 K. The blue tick marks correspond to nuclear reflections and the red tick marks to magnetic reflections. The shaded region contains a contribution from the cryostat and the vanadium sample holder and was excluded during the refinement.

References

[1] I. Yamada, M. Murakami, N. Hayashi, and S. Mori, *Inverse Charge Transfer in the Quadruple Perovskite CaCu3Fe4O12.*, Inorganic Chemistry **55**, 1715 (2016).

[2] D. Meyers et al., *Competition between Heavy Fermion and Kondo Interaction in Isoelectronic A-Site-Ordered Perovskites*, Nat Commun **5**, 5818 (2014).

[3] M.-R. Li et al., *Strong Electron Hybridization and Fermi-to-Non-Fermi Liquid Transition in $LaCu_3Ir_4O_{12}$*, Chem. Mater. **27**, 211 (2015).

[4] A. Collomb, D. Samaras, B. Bochu, and J. C. Joubert, *Propriétés et structure magnétiques de CaCu3Ti4O12 à structure pérovskite*, Phys. Stat. Sol. (a) **41**, 459 (1977).

[5] T. Saito, M. Toyoda, C. Ritter, S. Zhang, T. Oguchi, J. P. Attfield, and Y. Shimakawa, *Symmetry-Breaking 60°-Spin Order in the* A*-Site-Ordered Perovskite $LaMn_3V_4O_{12}$*, Phys. Rev. B **90**, 214405 (2014).

[6] M. Amano Patino et al., *Multi*-k *Spin Ordering in $CaFe_3Ti_4O_{12}$ Stabilized by Spin-Orbit Coupling and Further-Neighbor Exchange*, Phys. Rev. Research **3**, 043208 (2021).

[7] M. Amano Patino, F. Denis Romero, H.-J. Koo, M. Avdeev, S. D. A. Injac, M. Goto, M.-H. Whangbo, and Y. Shimakawa, *Orthogonal Antiferromagnetism to Canted Ferromagnetism in $CaCo_3Ti_4O_{12}$ Quadruple Perovskite Driven by Underlying Kagome Lattices*, Commun Mater **3**, 51 (2022).

[8] S. V. Ovsyannikov, Y. G. Zainulin, N. I. Kadyrova, A. P. Tyutyunnik, A. S. Semenova, D. Kasinathan, A. A. Tsirlin, N. Miyajima, and A. E. Karkin, *New Antiferromagnetic Perovskite $CaCo_3V_4O_{12}$ Prepared at High-Pressure and High-Temperature Conditions*, Inorg. Chem. **52**, 11703 (2013).

[9] S. V. Ovsyannikov et al., *Structural and Magnetic Transitions in $CaCo_3V_4O_{12}$ Perovskite at Extreme Conditions*, Inorg. Chem. **56**, 6251 (2017).

[10] S. Zhang, T. Saito, M. Mizumaki, W. Chen, T. Tohyama, and Y. Shimakawa, *Site-Selective Doping Effect in $AMn_3V_4O_{12}$ ($A = Na^+, Ca^{2+}$, and La^{3+})*, J. Am. Chem. Soc. **135**, 6056 (2013).

[11] B. H. Toby and R. B. Von Dreele, *GSAS-II : The Genesis of a Modern Open-Source All Purpose Crystallography Software Package*, Journal of Applied Crystallography **46**, 544 (2013).

[12] J. M. Perez-Mato, S. V. Gallego, E. S. Tasci, L. Elcoro, G. de la Flor, and M. I. Aroyo, *Symmetry-Based Computational Tools for Magnetic Crystallography*, Annu. Rev. Mater. Res. **45**, 217 (2015).

[13] H. Li, X. Liu, C. Li, S. Lv, Y. Bai, Z. Wang, and J. Meng, *Magnetic Coupling Mechanism in A-Site Ordered Perovskite $YMn_3Al_4O_{12}$: Extended (Mn–O)–(O–Mn) Superexchange*, Solid State Sciences **17**, 63 (2013).

[14] Y. Shimakawa and T. Saito, *A-Site Magnetism in A-Site-Ordered Perovskite-Structure Oxides*, Phys. Status Solidi B **249**, 423 (2012).

[15] N. L. Ross, J. Ko, and C. T. Prewitt, *A New Phase Transition in $MnTiO_3$:$LiNbO_3$-Perovskite Structure*, Phys Chem Minerals **16**, 621 (1989).

[16] N. I. Kadyrova, Yu. G. Zainulin, A. P. Tyutyunnik, N. V. Mel'nikova, and I. S. Ustinova, *High-Pressure/High-Temperature Synthesis, Crystal Structure, and Electrical Properties of CaCu3 − x Fe x V4O12*, Inorg Mater **47**, 1396 (2011).

[17] H. Shiraki, T. Saito, M. Azuma, and Y. Shimakawa, *Metallic Behavior in A-Site-Ordered Perovskites $AMn_3V_4O_{12}$ with A = Na+, Ca2+, and Y3+*, J. Phys. Soc. Jpn. **77**, 064705 (2008).

[18] S. Zhang, T. Saito, W.-T. Chen, M. Mizumaki, and Y. Shimakawa, *Solid Solutions of Pauli-Paramagnetic $CaCu_3V_4O_{12}$ and Antiferromagnetic $CaMn_3V_4O_{12}$*, Inorg. Chem. **52**, 10610 (2013).

[19] G. Zhang, Y. Wang, Z. Cheng, Y. Yan, C. Peng, C. Wang, and S. Dong, *A Class of Rare Antiferromagnetic Metallic Oxides: Double Perovskite $AMn_3V_4O_{12}$ ($A = Na^+, Ca^{2+}$, and La^{3+}) and the Site-Selective Doping Effect*, Phys. Chem. Chem. Phys. **17**, 12717 (2015).